# Polar vortex conditions during the 1995/96 Arctic winter: MLS ClO and $HNO_3$

M. L. Santee, G. L. Manney, W. G. Read, J. Froidevaux, and J. W. Waters
Jet Propulsion Laboratory, California Institute of Technology, Pasadena

Received ——— ; accepted ———

Short title: MLS ClO AND $HNO_3$ IN THE 1995/96 ARCTIC WINTER

**Abstract.** Microwave Limb Sounder (MLS) measurements of lower stratospheric ClO and $HNO_3$ during the 1995-96 Arctic winter are presented. The 1995-96 Arctic winter was both colder and more persistently cold than usual, leading to an enhancement in lower stratospheric ClO of greater magnitude, vertical extent, and duration than has been previously observed in the Arctic. Vortex concentrations of $HNO_3$ in mid-December were large due to diabatic descent. Trajectory calculations indicate that localized severe depletions of gas-phase $HNO_3$ in mid-February and early March did not arise from entrainment of midlatitude air into the vortex and were therefore presumably related to polar stratospheric cloud (PSC) formation. A strong correlation between temperature and gas-phase $HNO_3$ was evident, consistent with recurring PSC condensation and evaporation cycles in response to temperature fluctuations.

## Introduction

Significant interhemispheric differences in the severity of ozone depletion are attributed in large measure to underlying differences in seasonal temperature patterns and vortex behavior [*World Meteorological Organization (WMO)*, 1995]. The 1995-96 Arctic winter was both colder and more persistently cold than usual. Two upper tropospheric blocking ridge events led to lower stratospheric minimum temperatures that approached those of the Antarctic vortex. The 1995-96 Arctic winter meteorological conditions, and their influence on ozone destruction, are discussed by *Manney et al.* [this issue].

In this paper we examine the 1995-96 Arctic winter temperatures in relation to chlorine activation and the formation of polar stratospheric clouds (PSCs). Although direct observations of stratospheric aerosols inside the northern vortex are only occasionally available from Upper Atmosphere Research Satellite (UARS) instruments, profiles of gas-phase $HNO_3$ are now being obtained from the Microwave Limb Sounder (MLS) measurements [*Santee et al.*, 1995] and are used here to infer the presence of PSCs.

## Measurement Description

UARS MLS observations of lower stratospheric ClO have been presented previously for several northern and southern hemisphere winters [*Waters et al.*, 1993a, b, 1995; *Manney et al.*, 1996]. As reported by *Waters et al.* [1996], $HNO_3$ has a small effect on the ClO signal that was accounted for in the original retrieval algorithms by assuming climatological values. The Version 3 ClO values were biased high by as much as ~0.2 ppbv when $HNO_3$ departed substantially from climatology (e.g., under conditions of low gas-phase $HNO_3$ during PSC events). In addition, *Waters et al.* [1996] also report an 8% scaling error in the Version 3 ClO data arising from the use of an erroneous ClO line strength value. Both sources of error have been corrected in improved retrieval algorithms. Here we present new Version 4 ClO data, which have an estimated single profile precision and accuracy

of 0.4 ppbv and 10%/0, respectively, at 1( I hP:

The measurement of $HNO_3$ was not a primary MLS objective. However, there is a significant $HNO_3$ spectral feature, composed of many *R* branch rotational lines, which resides just outside the 205-GHz spectral region (MLS band 4) used to measure ozone. In the lower stratosphere, the pressure broadened line shape of this feature adds a weak slope to the ozone signal. Version 1 algorithms use this slope to retrieve profiles of gas-phase $HNO_3$, resulting in improved fits to the radiances. MLS $HNO_3$ measurements (from precursory algorithms) have been shown previously by *Santee et al.* [1995].

Preliminary validation studies indicate that the MLS $HNO_3$ data are scientifically useful 011 the 100, 46. and 22 hPa retrieval surfaces, where the estimated single-profile precisions are approximately 2.0. 3.0. and 4.5 ppbv, respectively. The estimated precisions are based 011 observed variability in a 11" roll% latitude band centered around the equator, where meteorological variability is expected to be small relative to the estimated retrieval error. Because natural atmospheric variation is not completely negligible, the true precisions may be slightly better than the estimates. These precisions are generally consistent with uncertainties estimated by propagating the radiometric noise through the retrieval algorithm. The estimated uncertainties, which are included in the MLS data files, are flagged negative under conditions of poor measurement sensitivity when the contribution from the a priori values (climatology) exceeds 25%. Thus quality control should be imposed on the $HNO_3$ data by discarding retrievals with negative uncertainty values.

Initial comparisons (over a limited data set) with colocated UARS Cryogenic Limb Array Etalon Spectrometer (CLAES) $HNO_3$ observations [*Kumer et al.*, 1996] show that the MLS $HNO_3$ agrees well at 100 hPa but is usually 0.2 ppbv lower at 46 hPa and 0-4 ppbv higher at 22 hPa (particularly in "chemical" regions). However, even where biases between the two data sets exist, there is good correspondence in the morphology of the CLAES and MLS $HNO_3$ fields.

## Analysis and Discussion

Maps of MLS ClO and gas-phase $HNO_3$ are presented in Figure 1 for selected days during the two 1995-96 northern winter north-viewing periods. Each map was produced by binning and interpolating spatially all data taken over a 24-hr period and interpolating to the 465 K potential temperature ($\theta$) surface using United Kingdom Meteorological Office (UKMO) temperatures. Contours of temperature and potential vorticity (PV) derived from the UKMO analyses are also shown. After the second week of December, 465 K minimum temperatures remained at or below 195 K [*Manney et al.*, this issue], the commonly-used threshold for the existence of Type I PSCs, until early March. Heterogeneous processing on the surfaces of PSC particles [e.g., *Solomon*, 1990] led to a substantial area of activated chlorine by mid-December; by late January, when north-viewing observations resumed, enhanced ClO filled most of the sunlit portion of the vortex.

Time series of area-weighted vortex averages of ClO at 465 K are shown in Figure 2 for the five northern winters of MLS measurements to date. To conserve the lifetime of the MLS scan mechanism, full vertical scans were performed only on selected days in the 1994-95 and 1995-96 northern winters. ClO enhancement in late December 1995 was greater than that in any of the previous UARS years, although only a limited amount of data were collected at this time in 1991. Vortex-averaged ClO in February 1996 was as high as ever previously observed in the Arctic, and the ClO remained enhanced for a longer duration. Both Version 3 and Version 4 ClO data are shown for 1995-96. Although the vortex averages from both datasets exhibit the same time evolution, the Version 3 values are larger due to the 8% line strength error and the contamination from the $HNO_3$ signal; as expected, the largest differences between the two versions occur on days for which the gas-phase $HNO_3$ values are lowest.

Significant ClO enhancement extended up to ~650 K in 1995-96, as shown in Figure 3. This exceeds the vertical range of enhanced ClO observed in previous Arctic

winters (for example, ClO was enhanced up to ~580 K in both 1992-93 [*Manney et al.*, 1994] and 1994-95 [*Manney et al.*, 1995]). The vertical extent of the ClO enhancement in February 1996 is similar to that typically seen in the Antarctic [*Manney et al.*, 1994], consistent with the larger vertical extent of Arctic ozone depletion in 1995-96 [*Manney et al.*, this issue].

Large concentrations of $HNO_3$ inside the vortex in mid-December (Figure 1) are attributed to diabatic descent. Between 29 and 30 January, 465 K gas-phase $HNO_3$ increased by approximately 3.1 ppbv on average over northern Scandinavia. Temperatures over this region, while remaining below 195 K, increased by about 1.3 K during this interval. In light of recent studies that have called into question the canonical model of Type I PSC formation, we have used the thermodynamic formula of *Hanson and Mauersberger* [1988] to calculate the vapor pressure of $HNO_3$ over nitric acid trihydrate (NAT) at 46 hPa. Using the observed temperatures and a $H_2O$ mixing ratio of 4.5 ppmv [*Kelly et al.*, 1990], we find the observed change in gas-phase $HNO_3$ (but not the actual mixing ratio values) to be consistent with that predicted by the *Hanson and Mauersberger* [1988] relationship.

A severe decrease in gas-phase $HNO_3$ occurred between 17 and 20 February, as temperatures dropped below 188 K between Greenland and Norway. The localized $HNO_3$ depletion extended up to 585 K and was confined to the area of low temperatures throughout its vertical range. As discussed by *Manney et al.* [this issue], a strong blocking ridge event in the upper troposphere at this time resulted in the deformation of the lower stratospheric vortex and the location of a region of very low temperatures near the vortex edge (see Figure 1). To investigate the cause of the $HNO_3$ decrease, high-resolution three-dimensional transport calculations, similar to those for ozone described by *Manney et al.* [this issue], were initialized using 465 K MLS $HNO_3$ on 30 January and run through 20 February. Comparison of the observations (Figure 1) with the results from the trajectory calculations (Figure 4a) indicates that the low values of 465 K gas-phase

$HNO_3$ on 20 February did not arise from entrainment of midlatitude air with smaller $HNO_3$ concentrations into the vortex associated with this tropospheric ridging event. A second (weaker) tropospheric blocking ridge occurred at the beginning of March [*Manney et al.*, this issue]. Another set of transport calculations was initialized on 24 February and run through 3 March. Again, the trajectory calculations (Figure 4b) show that the low $HNO_3$ values observed on 3 March (Figure 1) were not produced by intrusions of extra-vortex air during the second ridging event. The Halogen Occultation Experiment (11,41,010) 011 UARS detected high aerosol extinction indicative of a PSC at about 52°N and 0°E on 3 March (J. Russell, private communication, 1996). We conclude that the observed pockets of depleted gas phase $HNO_3$ resulted from PSC formation.

The relationship between temperature and observed gas phase $HNO_3$ is illustrated in Figure 5 for the second north-viewing winter period. The area-weighted averages were calculated from points enclosed within the 195 K temperature contour. Because of the occasionally significant differences between UKMO and U. S. National Meteorological Center (NMC) temperatures in the lower stratosphere and the sensitivity of gas-phase $HNO_3$ mixing ratios to small variations in temperature, the daily averages were computed using both UKMO and NMC temperatures. Similar results were obtained for both data sets. A strong correlation between temperature and gas phase $HNO_3$ is evident, suggesting recurring PSC condensation and evaporation cycles as the temperature fluctuates. Further studies are in progress to investigate how closely the behavior of MLS $HNO_3$ (and its correlation to temperature) conforms to that predicted by current models of PSC formation.

The MLS $HNO_3$ data alone do not allow us to distinguish between the temporary condensation of $HNO_3$ and the irreversible removal of $HNO_3$ through sedimentation of PSC particles (denitrification). However, Figure 1 shows signs of an overall decline in gas-phase $HNO_3$ within the vortex over the course of the winter. Calculation of daily $HNO_3$ vortex averages, excluding regions where the mixing ratio was less than 4 ppbv

(which are confined to the low-temperature regions and are likely due to the temporary sequestration of $HNO_3$ in PSC particles), reveals a decrease of 1 ppbv between 29 January and 3 March. This is suggestive of mild denitrification in the Arctic, in agreement with previous satellite, aircraft, and balloon based studies [e.g., *World Meteorological Organization (WMO)*, 1995; *Santee et al.*, 1996] that have found denitrification in the Arctic to be less severe than that in the Antarctic. Modeling of the effect of changing insolation on $HNO_3$ photochemistry and the replenishment of 465 K $HNO_3$ by transport processes is needed to verify this suggestion. The availability of a multi-year, global $HNO_3$ data set from MLS will facilitate more detailed comparisons of denitrification in the two hemispheres.

**Acknowledgments.** We would like to express our appreciation to our MLS colleagues, especially T. Lungu and L. Nakamura for their efforts in making the data available and R. P. Thurstans for graphics advice. We thank the NMC and the UK MO for meteorological data and C. Webster for helpful comments. Work at the Jet Propulsion Laboratory, California Institute of Technology, was done under contract with the National Aeronautics and Space Administration.

## References

Hanson, D., and K. Mauersberger, Laboratory studies of the nitric acid trihydrate: Implications for the south polar stratosphere, *Geophys. Res. Lett.*, *15*, 855-858, 1988.

Kelly, K. K., et al., A comparison of ER-2 measurements of stratospheric water vapor between the 1987 Antarctic and 1989 Arctic airborne missions, *Geophys. Res. Lett.*, *17*, 465-468, 1990.

Kumer, J. B., et al., Comparison of correlative data with $HNO_3$ version 7 from the CLAES instrument deployed on the NASA Upper Atmosphere Research Satellite, *J. Geophys. Res.*, *101*, 9621-9656, 1996.

Manney, G. L., et al., Chemical depletion of ozone in the Arctic lower stratosphere during winter 1992-93, *Nature*, *370*, 429-434, 1994.

Manney, G. L., et al., Arctic ozone depletion observed by UARS MLS during the 1994-95 winter, *Geophys. Res. Lett.*, *23*, 85-88, 1996.

Manney, G. L., M. L. Santee, L. Froidevaux, J. W. Waters, and R. W. Zurek, Polar vortex conditions during the 1995-96 Arctic winter: Meteorology and MLS ozone, *J. Geophys. Res.*, this issue.

Santee, M. L., et al., Interhemispheric differences in polar stratospheric $HNO_3$, $H_2O$, ClO, and $O_3$, *Science*, *267*, 849-852, 1995.

Solomon, S., Progress towards a quantitative understanding of Antarctic ozone depletion, *Nature*, *347*, 347-354, 1990.

Waters, J. W., et al., Stratospheric ClO and ozone from the Microwave Limb Sounder on the Upper Atmosphere Research Satellite, *Nature*, *362*, 597-602, 1993a.

Waters, J. W., L. Froidevaux, G. L. Manney, W. G. Read, and L. S. Elson, MLS Observations of lower stratospheric ClO and $O_3$ in the 1992 southern hemisphere winter, *Geophys. Res. Lett.*, *20*, 1219-1222, 1993b.

Waters, J. W., et al., UARS MLS observations of lower stratospheric ClO in the 1992-93 and 1993-94 Arctic winter vortices, *Geophys. Res. Lett.*, *22*, 823-826, 1995.

Waters, J. W., et al., Validation of UARS Microwave Limb Sounder ClO measurements, *J.*

*Geophys. Res.*, *101*, 10,091-10,127, 1996.

World Meteorological Organization (WMO), Scientific assessment of ozone depletion: 1994, *WMO Rep. 37*, Global Ozone Res. and Monit. Proj., Geneva, 1995.

This manuscript was prepared with the AGU LaTeX macros v3.1.

Figure 1. Maps of MLS ClO (left, ppbv) and $HNO_3$ (right, ppbv), for selected days during the two 1995-96 northern winter northviewing periods, interpolated to the 465 K potential temperature ($\theta$) surface using UKMO temperatures. The maps are polar orthographic projections extending to the equator, with the Greenwich meridian at the bottom and dashed black circles at 30°N and 60°N. No measurements were obtained in the white area poleward of 80°N. Other blank spaces in the maps represent areas where there were data gaps or spurious data points. Only data from the "day" side of the orbit are shown for ClO. Superimposed in white are the 0.25 x $10^{-4}$ and 0.30 x $10^{-4}$ $Km^2kg^{-1}s^{-1}$ contours of UKMO PV and in blue the 195 and 188 K contours of UKMO temperature.

**Figure 2.** Time series of area-weighted vortex averages of ClO at 465 K for five northern winters. The large data gaps in January/early February correspond to periods when MLS was viewing southern high latitudes; the smaller gap in early February 1996 corresponds to a period when the UARS spacecraft was not operational. Lower values of ClO are observed in mid-February/early March each year when there are essentially no daylight measurements due to precession of the orbit. Both Version 3 (filled cyan circles) and Version 4 (open cyan circles) data are shown for 1995-96; for all other years the data shown are Version 3.

**Figure 3.** Version 4 ClO abundances averaged over 18, 20 and 23 February (the days for which the 465 K ClO was highest), in PV/$\theta$ space. The PV axis is expressed in terms of equivalent latitude (the latitude enclosing the same area as a given PV contour).

**Figure 4.** 465 K $HNO_3$ (ppbv) from high-resolution trajectory calculations [*Manney et al.*, this issue]. The maps show the $HNO_3$ mixing ratios at the parcel positions on the initialization day advected with the parcels to their final positions. White spaces in the maps arise from data gaps on the initialization day. Two PV contours (see Figure 1) are overlaid in white. (a) Results on 20 February from calculations initialized with MLS $HNO_3$ data on 30 January. (b) Results on 3 March from calculations initialized with MLS $HNO_3$ data on 24 February.

**Figure 5.** Time series of area-weighted averages of temperature (red) and MLS $HNO_3$ (black) at 465 K, calculated within the area enclosed by the 195 K temperature contour. Results are shown using both UKMO (filled triangles connected by solid lines) and NMC (open squares connected by dotted lines) temperatures. NMC temperatures are missing on 16 and 21 February, and the gap in $HNO_3$ data in early February corresponds to a period when UARS was not operational.

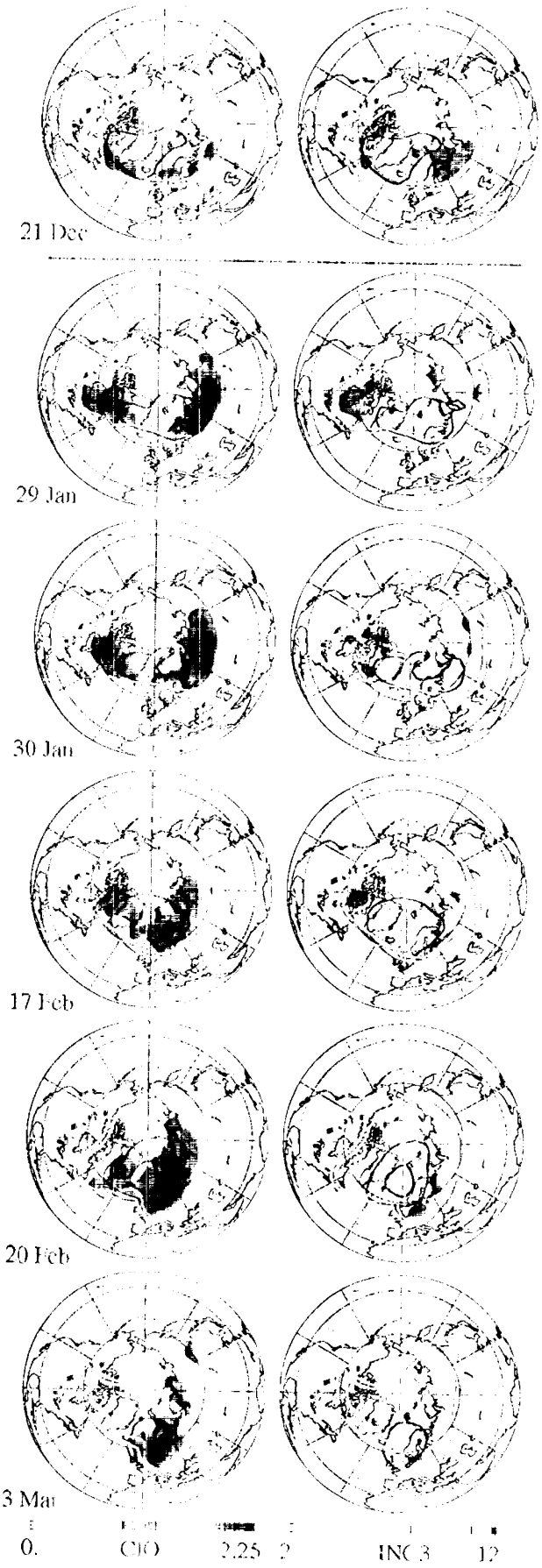


Figure 1

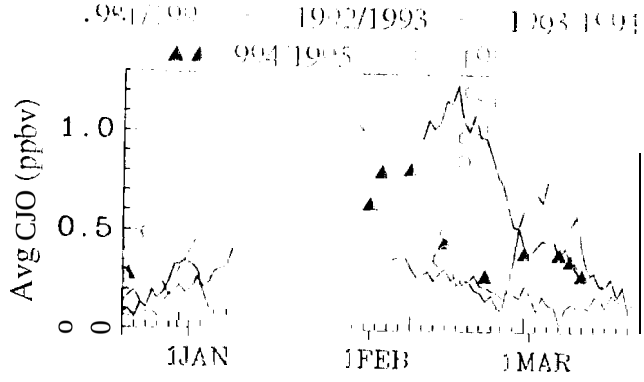


Figure 2

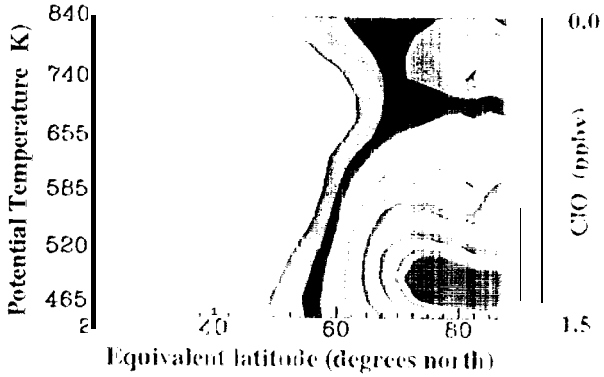
840
740
655
585
520
465
Potential Temperature (K)
20
60
80
Equivalent latitude (degrees north)
0.0
1.5
CIO (ppbv)

Figure 3

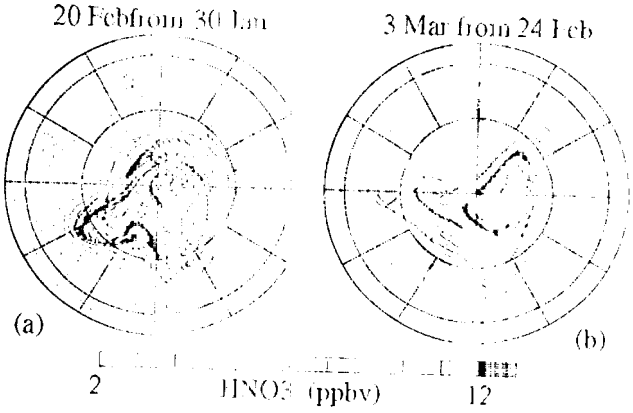


Figure 4

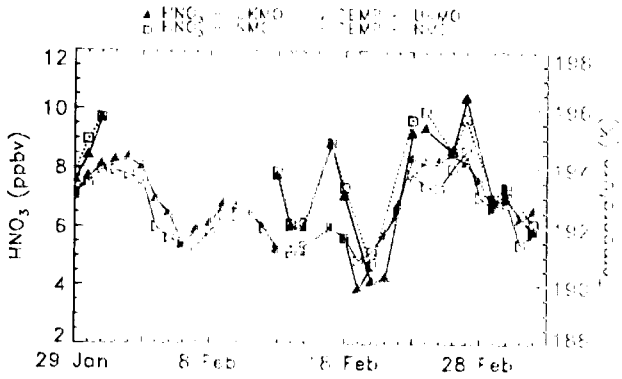


Figure 5